Different optical properties in different periodic slot cavity geometrical morphologies*

Jing Zhou(周静), Meng Shen(沈萌), Lan Du(杜澜), Caisong Deng(邓彩松), Haibin Ni(倪海彬), and Ming Wang(王鸣)†

Key Laboratory on Opto-Electronic Technology of Jiangsu Province, School of Physics Science and Technology, Nanjing Normal University, Nanjing 210023, *China*

(Received 18 January 2016; revised manuscript received 16 May 2016; published online 20 July 2016)

In this paper, optical properties of two-dimensional periodic annular slot cavity arrays in hexagonal close-packing on a silica substrate are theoretically characterized by finite difference time domain (FDTD) simulation method. By simulating reflectance spectra, electric field distribution, and charge distribution, we confirm that multiple cylindrical surface plasmon resonances can be excited in annular inclined slot cavities by linearly polarized light, in which the four reflectance dips are attributed to Fabry–Perot cavity resonances in the coaxial cavity. A coaxial waveguide mode TE11 will exist in these annular cavities, and the wavelengths of these reflectance dips are effectively tailored by changing the geometrical pattern of slot cavity and the dielectric materials filled in the cavities. These resonant wavelengths are localized in annular cavities with large electric field enhancement and dissipate gradually due to metal loss. The formation of an absorption peak can be explained from the aspect of phase matching conditions. We observed that the proposed structure can be tuned over the broad spectral range of 600–4000 nm by changing the outer and inner radii of the annular gaps, gap surface topography. Meanwhile, different lengths of the cavity may cause the shift of resonance dips. Also, we study the field enhancement at different vertical locations of the slit. In addition, dielectric materials filling in the annular gaps will result in a shift of the resonance wavelengths, which make the annular cavities good candidates for refractive index sensors. The refractive index sensitivity of annular cavities can also be tuned by the geometry size and the media around the cavity. Annular cavities with novel applications can be implied as surface enhanced Raman spectra substrates, refractive index sensors, nano-lasers, and optical trappers.

Keywords: cylindrical surface plasmons, finite difference time domain, Fabry–Perot cavity resonances, two-dimensional periodical structure

PACS: 73.20.Mf, 78.67.–n, 61.46.–w, 78.68.+m **DOI:** 10.1088/1674-1056/25/9/097301

1. Introduction

When light interacts with a metal, the cloud of free electrons in the metal can support a wave of charge density fluctuations on the surface of the metal. This phenomenon is called a surface plasmon wave.[1] Specific morphology of metal slit cavity will produce strong electric field enhancement. Surface plasmons can couple light strongly to the metal surface, which causes light to be confined in an area smaller than that predicted by the diffraction limit; and the local electromagnetic field intensity can be enhanced by many orders of magnitude, which can also be called nanocavity plasmons[2–4] and may have important implications in many optical sensing applications.[5,6] Such tunable optical properties depend strongly on the geometry of the metal structure itself, as a result of electrostatic interactions between confined electrons distributed over the surfaces of the metal conductor.

In recent years, cylindrical surface plasmons (a typical model of SPPs), which were called CSPs, excited in a nanoscale coaxial noble metals Au/Ag structure have generated great scientific interest.[7] These CSPs have been applied to nanoparticle plasmonic tweezers,[8] complex slits,[9] nanoantennas,[10,11] metallic groove arrays,[12] and oblique incidence unsymmetrical nanostructures.[13,14] In order to explore the relationship between the parameters and CSP modes, previous investigators were concerned more about the vertical equivalent cavity length and the horizontal width of the slit gap.[15,16] Meanwhile, some works concentrated on changing the angle of incident light.[17,18] However, few studies focused more elaborate appearance characteristics on the cavity resonance modes, such as the tilt angle of the inner/outer cavity, or the sag degree of the cavity wall through a specific parameter calibration.

In this paper, a model of two-dimensional periodic annular slot cavity arrays in hexagonal close-packing on a silica substrate is calculated by finite difference time-domain method.[19,20] It is explored that different parameters have different influence on the cavity modes. On one hand, we verify that with the increase of gap width, the dip-wavelength red shifts in certain rules based on the theory of Fabry–Perot cavity resonances. The relevant detailed reasons have already been reported in Ref. [21]. On the other hand, we concentrate on the pattern characteristic of ring cavities and their refractive index of the surroundings. It is found that a specific pattern

*Project supported by the National Natural Science Foundation of China (Grant No. 61178044), the Natural Science Foundation of Jiangsu Province, China (Grant No. BK20160969), and the University Postgraduate Research and Innovation Project of Jiangsu Province, China (Grant No. KYLX_0723).

†Corresponding author. E-mail: wangming@njnu.edu.cn

© 2016 Chinese Physical Society and IOP Publishing Ltd

characteristic may result in a directed shift of the SPP dips toward longer wavelengths. The physical mechanism of plasmon shifting can be illustrated by the Coulombic interaction from the charges at the interfaces of metal nanoparticle. The excellent optical properties can bring various possible applications to microns/nano optical device research, such as, ultrasensitive detection,[22] integrated optical components, and bio-chemical sensors.[23,24]

2. Simulation model and calculation method

In the previous work, we have already studied the physical mechanism of a hexagonal close-packing silver cap model.[21] In this paper, we design a precise cylindrical slot cavity, and the geometric parameters of this cavity can be adjusted more accurately. Large enhancement of local electric field distribution exists in the slot cavity, and the resonance dips can be better controlled due to the easy adjusting of the cavity angle. Longer cavity length makes more modes restricted in the cavity than the previous one, and the refractive index of sensitivity is significantly improved when applied to the refractive index sensor.

The proposed two-dimensional periodic annular slot cavity arrays in hexagonal close-packing on a silica substrate are shown in Fig. 1(a), and the cross section of a single structure with the light paths through it is shown in Fig. 1(b). The inner and outer radii of the annular cavity gaps, the vertical height of the cavity, the bottom silver layer thickness, and the upper convex silver layer thickness are denoted by r, R, L, h, and a, respectively. The annular slot cross section is constrained by θ and φ. The period $p = 690$ nm. The structural parameters are defined as: $r = 210$ nm, $R = 229$ nm, $L = 500$ nm, $\theta = 89°$, $\varphi = 90°$, $h = 185$ nm, and $a = 100$ nm. The dielectric constant of glass substrate silica is 2.37. Numerical simulations by the finite difference time domain (East FDTD, Dong Jun technology, Shanghai, China) are proposed. We model the dielectric constant of Ag with an extended Drude model.[25] Annular inclined slot cavities which have the positive surface are arranged on the silica substrate in hexagonal close-packing. The transverse magnetic (TM) polarized Gaussian pulse with the extended source type of Gauss window light irradiates the arrays at an incident angle of 0 (illuminated by a y-axis directional polarized incident field with its wave vector k along the negative x-axis). In order to confirm the simulation is computationally feasible, the mesh grid size ($\Delta x = 5$ nm, $\Delta y = 5$ nm, $\Delta z = 5$ nm), calculation steps ($\Delta = 100000$ steps) and the time step ($\Delta t = 83.391$ fs) are set to satisfy the Courant stability condition.[20] The two horizontal directions (y axis and z axis) are in periodic boundary conditions and the x axis is in PML boundary conditions to ensure the dielectric of the boundary continuously.

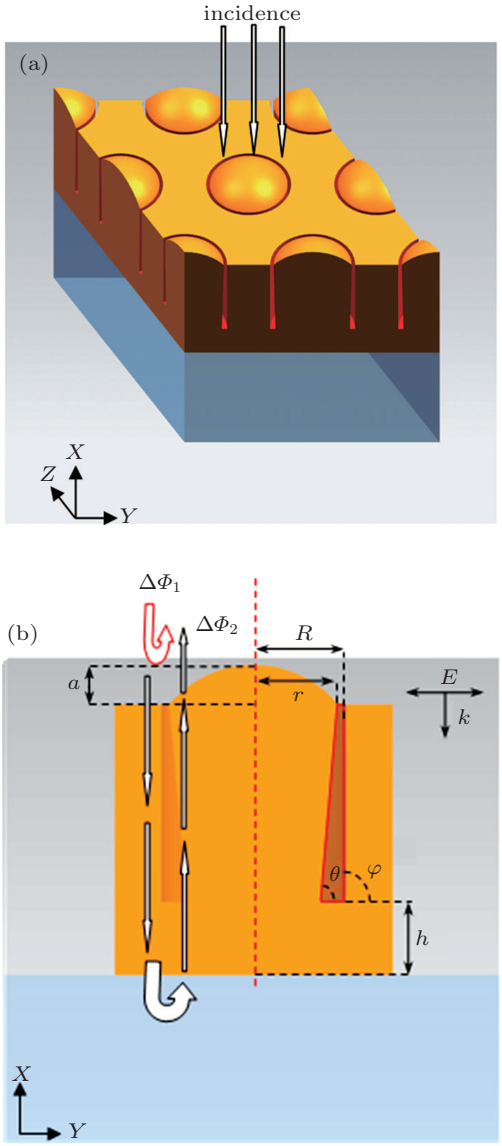


Fig. 1. (color online) (a) Schematic of the cavity-coupled plasmonic structure and (b) cross section diagram of a single structure with the light paths through it.

3. Results and discussion

3.1. Reflectance spectra and local electric field distribution of annular slot cavity arrays

The reflectance spectra of the periodic annular inclined slot cavity arrays are shown in Fig. 2(a). We confirm that multiple cylindrical surface plasmon resonances result in four apparent reflectance dips (denoted as $J_1 = 2120$ nm, $J_2 = 1164$ nm, $J_3 = 776$ nm, and $J_4 = 630$ nm). They can be excited in annular cavities by linearly polarized light. The reflectance spectra consisting of a single annular cavity cell and annular cavity arrays are shown in Fig. 2(b). The normalized reflectance of the single cell is about ten percent of the reflectance of annular cavity arrays. Meanwhile, the electric field intensity of a single slit resonant cavity structure relative to the periodic structure is weak,[21] but it still persists with four obvious dips, almost the same as the periodic structures. The reasons for this phenomenon can be illustrated from a sin-

gle circular cavity dimension to the formation of absorption dips, as certain related articles have reported.[26–29] The CSPs that exist in TM modes with the field enhancement will be excited on cylindrical metal–dielectric interfaces on account of the negative dielectric constant of the metal silver. According to the theories of single waveguide cavity,[30] only the TE11 modes that meet the phase matching conditions may exist in the air cavity by the irradiation of linear polarized light, according to the following equations:

$$|2Lk_{\mathrm{SPP}}(\omega)+\Delta\varphi_1+\Delta\varphi_2|=2\pi m, \tag{1}$$

where L is the length of the cavity, $k_{\mathrm{SPP}}(\omega)$ the wave vector of the plasmon at frequency ω, $\Delta\varphi_{1,2}$ the phase shifts of plasmon reflection at the upper and bottom of the cavity, and m the mode number (different measured resonance symbols). Certain specific wavelengths (J_1, J_2, J_3, and J_4) of incident light satisfy Eq. (1). The field profile in the cavity is a propagating superposition of plasmon waves propagating. The field profile is simply proportional to the original plasmon wave and the plasmon wave after one reflection, added together. The electric field in the cavity as a function of position in the direction parallel to the waveguide axis is given by

$$E(z)\propto \mathrm{e}^{\mathrm{i}kz}+|r_1|\,\mathrm{e}^{\mathrm{i}[k(L-Z)+<K>L+\Delta\varphi_1]}, \tag{2}$$

where k is the plasmon wave vector, $\langle k\rangle$ is the index-averaged wave vector, $|r_1|$ and $\Delta\varphi_1$ are the reflectance and reflection phase shift at the distal end of the cavity, respectively. To investigate the origin of those four resonance dips, electric field distributions and charge intensity of the four pronounced plasmon resonances (excited at the wavelength of J_1, J_2, J_3, and J_4) in the vertical cross section, which is parallel to the polarization direction of the incident light, are presented in Fig. 2(c). The horizontal electric field distributions and charge intensity cross sections at the locations of the identified dotted line are shown in Fig. 2(d). Apparently, a strong steady-state electric field enhancement (at the resonance dip wavelength) which is attributed to Fabry–Perot cavity resonance, results from interference between forward and backward propagating plasmon waves existing in the coaxial cavity gaps. These local field enhancements arising from the sharp edges make these nanostructures ideal platforms for SPP applications.

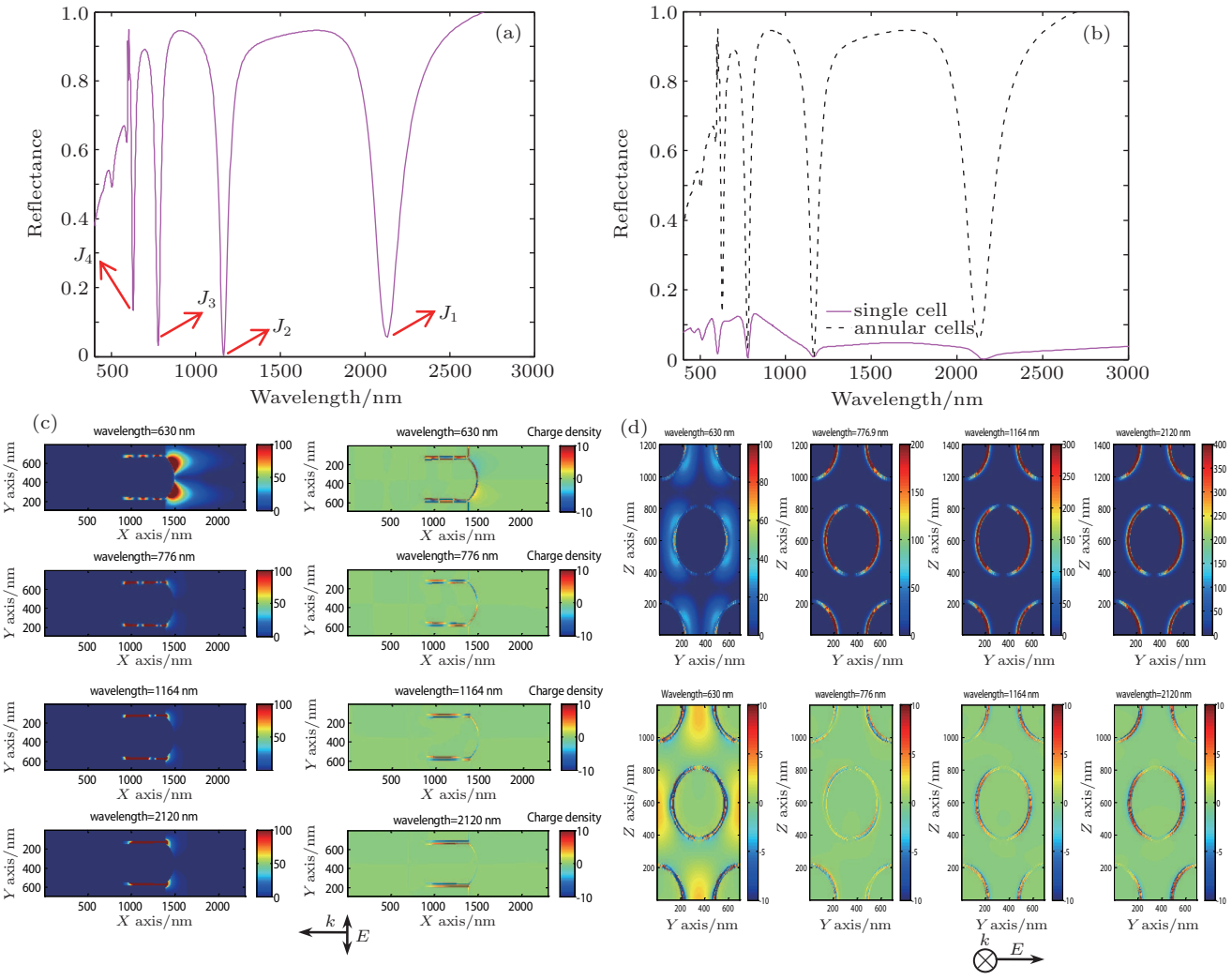


Fig. 2. (color online) (a) Calculated reflectance spectra with four resonance dips. (b) Reflectance spectra of a single annular cavity cell and annular cavity arrays with the same geometry size. (c) Vertical schematic cross section of electric field distributions and charge density distributions at resonance wavelengths. (d) Horizontal schematic cross section of electric field distributions and charge density distributions at resonance wavelengths.

3.2. New SPP modes in specific cavity arrays

When these nanostructure cavities are hollow (ii) and filled with silica dielectric (iii), their vertical cross section is shown in Fig. 3(a). By comparing the air-filled hollow slit cavity and silica-filled cavity with the original one (i), we show their reflectance spectrum in Fig. 3(b), where two more reflectance dips show up. According to Eq. (1), L is defined by optical distance, which not only represents the absolute height of the slit cavity, but also is constrained by the cavity-filled medium. The dispersion increases by virtue of the change of medium refractive index that results in two more resonance modes. It is concluded that the silica dielectric layer constrained more wave pattern, and the specific frequency electromagnetic waves lost in the cavity. Furthermore, more modes which meet the resonance condition were transmitted through the hollow cavity. In a word, the fact that the surface plasmon resonance on the surface of the metal film results in new resonance modes is the main reason for the added SPP-dips.[26]

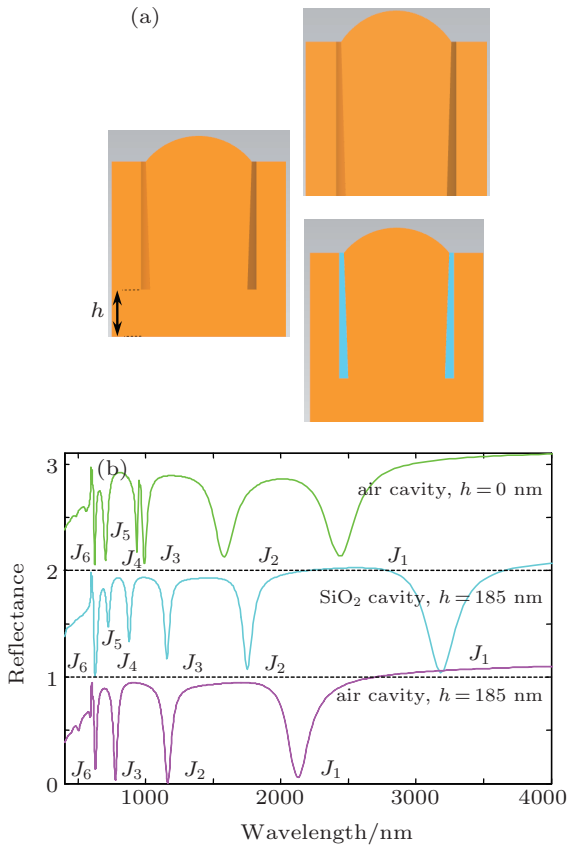


Fig. 3. (color online) (a) Schematic cross section of air-filled cavity, hollow slit cavity, and silica-filled cavity. (b) Reflection spectrum comparison of air-filled cavity and silica-filled cavity structure.

3.3. Principles of tunable SPPs in different air cavities

3.3.1. Tunable SPPs by varying outer radii R, inner radii r, and cavity length L

The parameters' variation of outer radii R, inner radii r, and cavity length L is conformed with the theory of Fabry–Perot resonance. In order to meet the coaxial waveguide boundary conditions, the change of inner diameter r and outer diameter R will cause the TE11 mode to change. According to Eq. (1), we obtain the resonance frequency as a function of L, so changing the cavity length will lead to the resonance wavelength change.

It is found that SPP modes will change with the variation of the outer diameter, inner diameter, and the length of the air-filled cavity, and each parameter varies independently. Figure 4(a) shows the reflectance spectra with inner radius $r = 210$ nm, and outer radius R increases from 229 nm to 289 nm in 20 nm increments. Discussion is focused on the dip J_1 ($m = 1$), the slit gap gets widened when R increases gradually, and the resonance dip wavelength at 2120 nm for $R = 229$ nm gradually blue shifts to 1573 nm for $R = 289$ nm. Keep the outer radius $R = 229$ nm, and the inner radius changes from 150 nm to 210 nm with the increment of 20 nm. The gap width is narrower, note that the J_1 mode shows a red-shift from 1321 nm to 2120 nm with 799 nm wavelength growth, but increasing R just leads to 547 nm wavelength decrease. That is to say, changing r is more conducive to the resonance dips shifting, and the propagating CSP's on each of the metal–dielectric interfaces become strongly coupled when the ring narrows. Also, phenomenon on J_1–J_4 shows that both increasing R and decreasing r may lead to the reflectance-dip red shift, because the wave functions of CSPs overlap more efficiently. Meanwhile, the increase of gap width will make resonance dips show various significant characteristics. The dip will broaden when decreasing R, but may not broaden obviously when changing r.

Figure 4(c) shows reflectance spectra of 19 nm wide coaxial slot cavities with length increasing from 300 nm to 700 nm (same as Fig. 1(b)) in 100-nm increments. Several features are observed. At the lowest order ($m = 1$), the resonance wavelength 2254 nm for the longest cavity ($L = 700$ nm) gradually blue-shifts to 1813 nm for the shortest cavity ($L = 300$ nm). At the higher order ($m = 2$), resonance wavelength at 1421 nm for the largest cavity length blue-shifts to a wavelength at 833 nm for cavity length at 300 nm. Furthermore, the resonance dips in the higher-order ($m = 3, 4, 5$) wavelength range of the spectra also blue-shifts when the length of the cavity is decreased. The lowest-order resonances observed in the short cavity appear to be much broader than other resonances. This is possibly the result of a longer-wavelength resonance that arises when all propagating modes in the resonator are in cutoff.

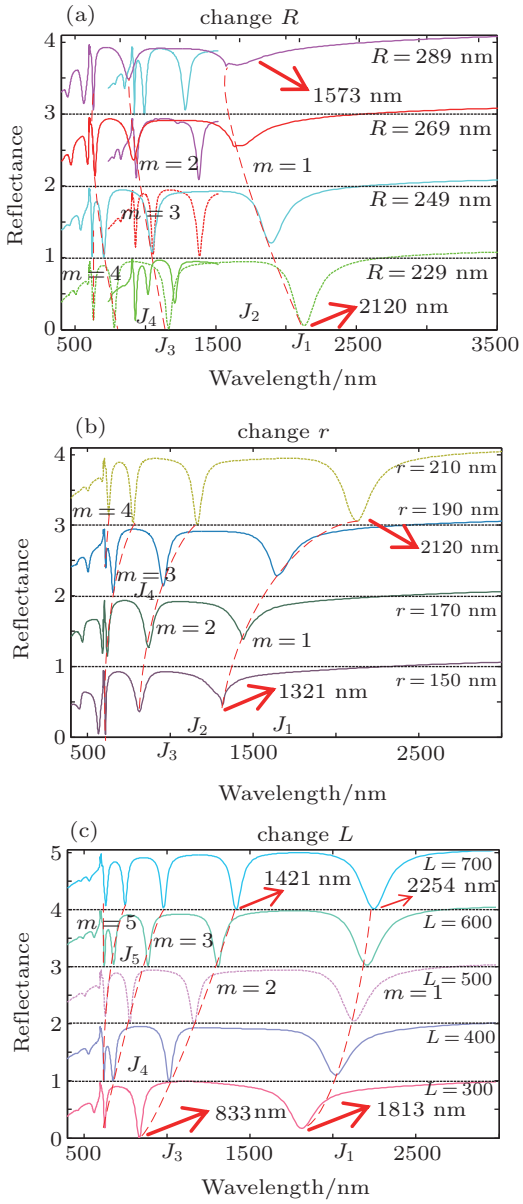


Fig. 4. (color online) Comparison of reflectance spectra for coaxial cavity by (a) varying inner radius r, (b) varying outer radius R, and (c) cavity length L. Data are shifted vertically for clarity. The red dashed lines are guides for the eye and connect the resonance dips ($m = 1, 2, \ldots$).

3.3.2. Tunable SPPs by changing parameter θ, θ', and cylindrical silver lateral bending radius t

Two methods were presented to describe the detailed shape of the slit. One is changing the gap angle at the bottom of the cavity by varying parameter θ ranging from 85°–90° (cross section shown in Fig. 5(b)), and θ' ranging from 90°–95° (cross section shown in Fig. 5(c)). The other way is changing the columnar silver bending radius t which represents the biggest distance of cavity slit (line scale of segment BD). As shown in Fig. 5(d), parameter t increases from 4 nm to 39 nm, with a step of 5 nm. Point B is the halfway point of the arc ABC, and point D is the halfway point of the line segment EF.

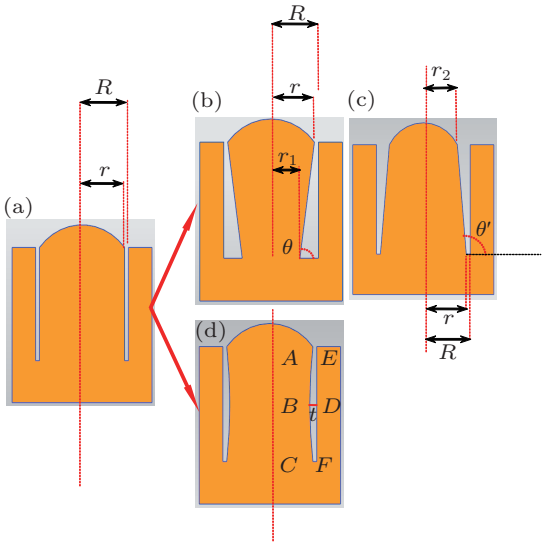


Fig. 5. (color online) Cross section of coaxial cavity with: (a) vertical slit, (b) inclined slit defined by θ, and (c) inclined slit defined by θ', (d) bending radius t. The middle convex silver is defined as columnar, as shown in Fig. 4(a), R–$r = 19$ nm.

We observed that r_1 increases with the increase of θ, and r_2 decreases with the increase of θ'. Parameters r_1 and r_2 calibrate the gap size at the beginning and the ending of the slit cavity. That is, increasing θ and θ' leads to reducing the bottom cavity gap width and enlarging the top cavity gap width, differently. The spectral reflectance contrast by varying θ and θ' is shown in Figs. 6(a) and 6(c). Figures 6(b) and 6(d) describe the relationships between wavelengths of reflectance dip (J_1–J_4) and geometry sizes (θ and θ'). The four dip wavelengths red-shift with the increase of θ and the decrease of θ'. We mainly notice that the resonance dip $J_4 = 1965$ nm for $\theta = 85°$ gradually red-shifts to 2195 nm for $\theta = 90°$, and the resonance dip J_4 at 2195 nm for $\theta = 90°$ gradually blue-shifts to 1525 nm for $\theta = 95°$. It is concluded that changing the gap width may result in the blue shift of the resonance dips, both at the beginning and the ending of the cavity. According to the approximate linear fitting relationship between θ/θ' and wavelength, $\Delta\lambda/\Delta\theta = 46$, $\Delta\lambda/\Delta\theta' = 134$, the upper shape of the slit cavity has a greater influence on the resonance-dip shift than the bottom. To further understand the physical mechanism, electric field distributions and charge density distributions at resonance wavelength 2195 nm of the vertical structure is simulated in Fig. 6(e). Local electric field enhancement concentrated at the top of the slit cavity is stronger than the bottom.

We consider the effect of middle bending radius on the absorption dip wavelength. The comparison of spectral reflectance is shown in Fig. 6(f), and relationship between resonance dip wavelength and t are shown in Fig. 6(g). J_1, J_2, J_3, J_4 blue shift as t increases from 9 nm to 29 nm, with a step of 5 nm. $\Delta\lambda/\Delta t = 40.5$, the dip wavelength shifts 40.5 nm, while the middle gap width changes every nanometer.

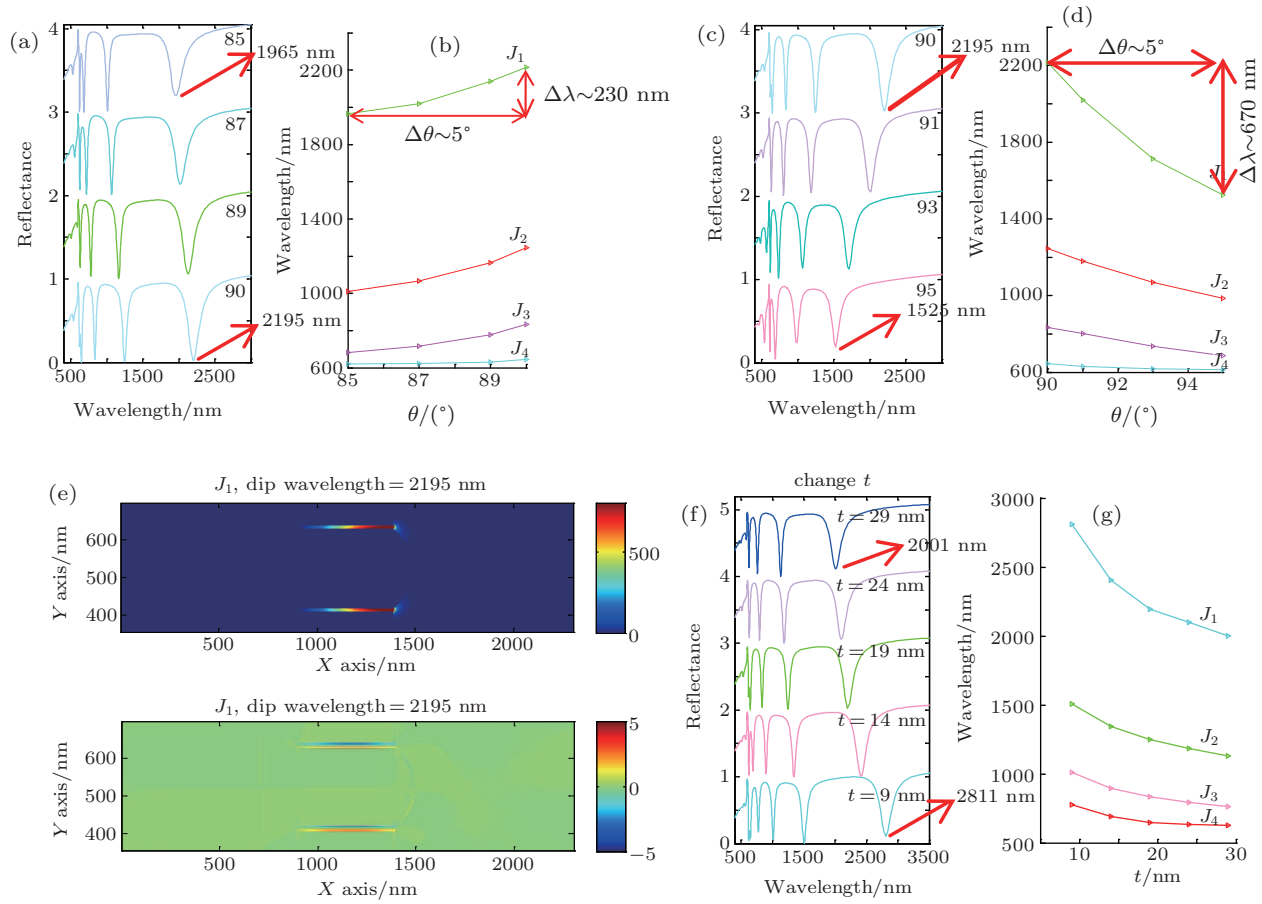


Fig. 6. (color online) Comparison of reflectance spectra of annular cavity array with (a) decreased θ, (b) relationship between resonance dip wavelength and θ, (c) decreased θ', (d) relationship between resonance dip wavelength and θ'. (e) Cross section of electric field distributions and charge density distributions at a resonance wavelength of 2195 nm. Comparison of reflectance spectra of annular cavity array with (f) increased t, and (g) relationship between resonance dip wavelength and t.

3.4. Tunable SPPs by varying refractive indices in the cavities

According to Eq. (1), when the cavity is filled in the homogeneous medium, 'L' represents optical distance. It is not only related to the absolute height of the gap, but also relevant to the refractive indices in the cavities. To further investigate the tunability of the reflectance of cavity-filled media and the corresponding resonance dips, simulations are concentrated on four different filled media in cavity: water, propanol, olive, and benzene. Their refractive index is 1.3333, 1.3593, 1.4763, and 1.5012, respectively. The four dips red-shift as the refractive index of filling medium increases, which are shown in Fig. 7(a). Meanwhile, relationships between wavelengths of dips (J_1, J_2, J_3, J_4) and refractive indices of infiltrated liquids are almost linearly dependent, which is shown in Fig. 7(b). In summary, the dip wavelength changes relative to the filled media in slit cavity, and the sensitivity can be as high as 2100 nm/RIU when applied as a refractive index sensor.

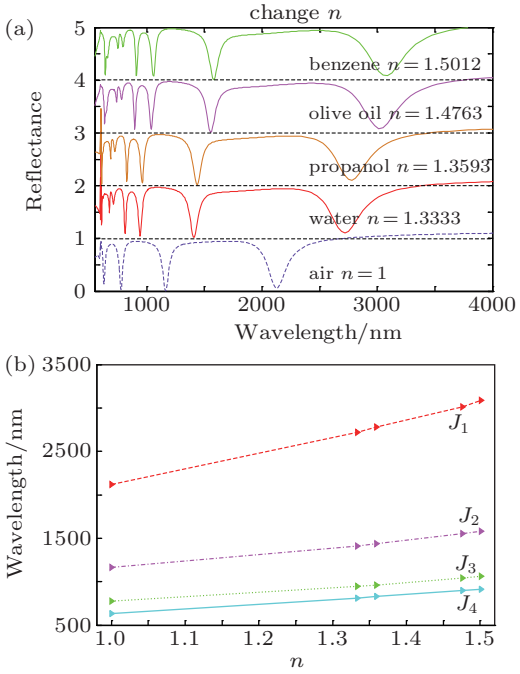


Fig. 7. (color online) (a) Reflectance spectra of annular cavity arrays with liquids of different refractive indices infiltrated in the cavities. (b) Relationships between wavelengths of dips J_1–J_4 and refractive indices of infiltrated liquids.

4. Conclusion

In conclusion, optical properties of periodic annular slit cavity arrays depending on surface plasmon resonances and local field enhancement have been investigated numerically. Our simulation results agree well with the model and demonstrate high tunability by changing the coaxial cavity gap and dielectric medium, which correspond to the theory of Fabry–Perot cavity resonance. The transmission of single cavity was compared with that of the period cavity arrays, and the tunability of SPP modes was adjusted by filled silica cavity and hollow slit cavity. The study was focused on the effect of size of a slit cavity at different positions on absorption dip-wavelength. Our work is helpful for understanding the physical origin of the unit plasmon resonance modes in special slit morphology. The high sensitivity of this structure may open the way to realization of plasmonic cavities with ultrasmall mode volumes, being a superior refractive index sensor in future.

References

[1] Stefan A M 2007 *Plasmonics: Fundamentals and Applications* (Germany: Springer) pp. 65–87

[2] Huang F M, Wilding D, Speed J D, Russell A E, Bartlett P N and Baumberg J J 2011 *Nano Lett.* **11** 1221

[3] Wang Q Y, Wang J and Zhang S L 2008 *Opt. Express* **16** 19882

[4] Cole R M, Baumberg J, Garcia de Abajo F J, Mahajan S, Abdelsalam M and Bartlett P N 2007 *Nano Lett.* **7** 2094

[5] Li J Y, Qiu K S and Ma H Q 2014 *Chin. Phys. B* **23** 106804

[6] López-Tejeira F, Rodrigo S G, Martín-Moreno L, García-Vidal F J, Devaux E, Ebbesen T W, Krenn J R, Radko I, Bozhevolnyi S I and González 2007 *Nat. Phys.* **3** 324

[7] Nordlander P and Prodan E 2004 *Nano Lett.* **4** 899

[8] Chen J J, Kang Z W, Lu H F, Zhang H X, Choy W C H, Chen N K and Ho H P 2015 *Vacuum* **118** 171

[9] Zhang X, Li Z, Chen J, Yue S and Gong Q 2013 *Opt. Express* **21** 14548

[10] Liao H M, Li Z, Chen J J, Zhang X, Yue S and Gong Q H 2013 *Sci. Rep.* **3** 1918

[11] Liu Y, Palomba S, Park Y, Zentgraf T, Yin X B and Zhang X 2012 *Nano Lett.* **9** 853

[12] Huang X P and Brongersma M L 2013 *Nano Lett.* **11** 5420

[13] Sonnefraud Y, Kerman S, Di Martino G, Lei D Y and Maier S A 2012 *Opt. Express* **5** 4893

[14] Lu F, Xiao F, Li K and Xu A 2014 *Opt. Lett.* **11** 3254

[15] Baida F I, Belkhir A, Van Labeke D and Lamrous O 2006 *Phys. Rev. B* **74** 205419

[16] Fan W, Zhang S, Minhas B, Malloy K J and Brueck S R J 2005 *Phys. Rev. Lett.* **94** 033902

[17] Zhou W, Dridi M, Suh J Y, Kim C H, Co D T, Wasielewski M R, Schatz G C and Odom T W 2013 *Nat. Nanotechnol.* **99** 506

[18] Huang F M, Wilding D, Speed J D, Russell A E, Bartlett P N and Baumberg J J 2011 *Nano Lett.* **11** 1221

[19] Gedney S D 1996 *IEEE Trans. Antennas. Propagat.* **44** 1630

[20] Ge D B and Yan Y B 2002 *Finite-Difference Time-Domain Method for Electromagnetic Waves* (Xi-an: Xi-an University of Electronic Science and Technology Press)

[21] Zhou J, Wang M, Ni H B and Ma X 2015 *Acta Phys. Sin.* **64** 227301 (in Chinese)

[22] Liu X J, Cao L Y, Song W, Ai K and Lu L H 2011 *Appl. Mater. Interf.* **3** 2944

[23] Huang C J, Ye J, Wang S, Stakenborg T and Lagae L 2012 *Appl. Phys. Lett.* **100** 173114

[24] Im H, Bantz K C, Lee S H, Johnson T W, Haynes C L and Oh S H 2013 *Adv. Mater.* **25** 2678

[25] Castella H, Zotos X and Prelovšek P 1995 *Phys. Rev. Lett.* **74** 972

[26] Waele R D, Burgos S P, Polman A and Atwater H A 2009 *Nano Lett.* **9** 2832

[27] Michael I H, Carl S and Grish B 2006 *Appl. Phys. Lett.* **88** 193104

[28] Fan W, Zhang S, Minhas B, Malloy K J and Brueck S R J 2005 *Phys. Rev. Lett.* **94** 033902

[29] Ni H B, Wang M, Shen T Y and Zhou J 2015 *ACS Nano* **9** 1913

[30] Haftel M I, Schlockermann C and Blumberg G 2006 *Phys. Rev. B* **74** 235405